

Hydrodynamic models of pulsation period evolution in R Hydrae

Yuri A. Fadeyev,^{1*}

¹*Institute of Astronomy, Russian Academy of Sciences, 119017, Pyatnitskaya str., 48, Moscow, Russia*

Accepted XXX. Received YYY; in original form ZZZ

ABSTRACT

Pulsation period evolution during the helium–shell flash in the Mira variable R Hya is investigated using consistent stellar evolution and non–linear stellar pulsation computations. The initial and time–dependent inner boundary conditions for the equations of radiation hydrodynamics describing non–linear stellar oscillations were determined using a grid of TP–AGB model sequences with initial masses on the main sequence $1.5M_{\odot} \leq M_{\text{ZAMS}} \leq 5.0M_{\odot}$ and the initial metallicity $Z = 0.014$. The setup of initial conditions for hydrodynamic models corresponds to ≈ 100 yr prior to the maximum of the helium–shell luminosity and ensures that the stellar envelope of the evolution model is under both hydrostatic and thermal equilibrium. Solution of the equations of hydrodynamics allowed us to determine the temporal variation of the pulsation period $\Pi(t)$ during ≈ 500 yr. Within this time interval R Hya is a fundamental mode pulsator. The period temporal dependencies $\Pi(t)$ calculated for the AGB star models at the beginning of the third dredge–up phase and with masses $4.4M_{\odot} \lesssim M \lesssim 4.5M_{\odot}$ are in agreement with observational estimates of the period of R Hya obtained during last two centuries. The mean radius of R Hya pulsation models at the end of the XX century ($470R_{\odot} \lesssim \bar{R} \lesssim 490R_{\odot}$) agrees with observational estimates obtained using the interferometric angular diameter measurements.

Key words: hydrodynamics – stars: evolution – stars: oscillations – stars: late-type – stars: individual: R Hya

1 INTRODUCTION

First observations of R Hya were conducted by Hevelius in 1662 and Montanary in 1670 (Argelander 1869), whereas discovery of variability is attributed to Maraldi in 1704 (Müller & Hartwig 1922). Regular observations of R Hya were started in the middle of XIX century and great attention to this variable star was attracted due to detection of the decreasing period of its light variations (Gould 1882). Period decrease in R Hya was reviewed by Chandler (1896) and Prager (1936) but the most recent and comprehensive analysis of period changes can be found in the paper by Zijlstra et al. (2002). In particular, Zijlstra et al. (2002) showed that the stage of period decrease lasted from around 1770 when the star oscillated with the period $\Pi_a^* \approx 480$ d to nearly 1950 when the period reduced to $\Pi_b^* \approx 380$ d. Thus, at present R Hya is the only Mira–type variable star with observational estimates of the period decrease time interval $\Delta t_{ab}^* \approx 180$ yr as well as the period values Π_a^* and Π_b^* at the endpoints of this interval.

R Hya is a Mira–type pulsating variable star (Samus’ et al. 2017) with absorption spectrum of class M6e (Merrill 1946, 1952, 1957) corresponding to a surface carbon to oxygen abundance ratio $C/O < 1$. At the same time detection of absorption lines of the radioactive element technetium (Tc I) shows that R Hya is a thermally pulsing AGB star experienc-

ing the third dredge–up (Orlov & Shavrina 1984; Little et al. 1987; Lebzelter & Hron 2003). According to the evolutionary calculations of Wood & Zarro (1981) the period decrease in R Hya is due to changes of the stellar radius and luminosity accompanying the helium–shell flash. Unfortunately, no detailed stellar pulsation calculations for R Hya models have been done so far so that the mass of R Hya still remains unclear.

The period of radial oscillations and the stellar radius relate as $\Pi \propto R^{3/2}$ therefore some qualitative considerations about period change can be obtained from temporal variations of the stellar radius. A helium–shell flash is accompanied by two consecutive phases of declining stellar radius and luminosity (Wood & Zarro 1981; Iben 1982; Boothroyd & Sackmann 1988). The onset of the first stage nearly coincides with the maximum peak of the helium–shell luminosity $L_{3\alpha}$ when the hydrogen–burning shell rapidly extinguishes (Fadeyev 2022). The stellar contraction ceases as soon as the radiation–diffusion wave from the helium–shell flash propagates up to the outer convection zone. The duration of the first radius decline Δt_1 is several dozen times shorter than that of the second radius decline Δt_2 and both these time scales decrease with increasing mass of the degenerate carbon core. In particular, for AGB stars with initial masses $1.5M_{\odot} \leq M_{\text{ZAMS}} \leq 5M_{\odot}$ these time intervals are in the range $10 \text{ yr} \lesssim \Delta t_1 \lesssim 300 \text{ yr}$ and $150 \text{ yr} \lesssim \Delta t_2 \lesssim 1.5 \times 10^4$, respectively.

* E-mail: fadeyev@inasan.ru

A first goal of the present work is to determine the evolutionary sequence with radius decline responsible for the pulsation period decrease observed in R Hya. In particular, we look for a model with the pulsation period at the onset of radius decline $\Pi \approx 480$ d and the duration of following period decrease ≈ 180 yr. The second goal of this work is that the selected evolutionary sequences are used for construction of hydrodynamic models describing the evolution of the pulsation period so that results of hydrodynamic computations can be compared with observations of the period in R Hya obtained in the last two centuries. To this end we compute the non-linear stellar pulsations using the time-dependent inner boundary conditions determined from the evolutionary calculations. This method has been earlier employed for modelling the pulsation period decrease in the Mira-type variable T UMi (Fadeyev 2022).

2 STELLAR EVOLUTION CALCULATIONS

The present study is based on calculations of the stellar evolution from the main sequence up to the AGB tip. Selected models of evolutionary sequences were used to determine the initial and time-dependent inner boundary conditions for the equations of radiation hydrodynamics describing radial stellar oscillations. We considered several evolutionary sequences with masses on the main sequence $1.5M_{\odot} \leq M_{\text{ZAMS}} \leq 5.0M_{\odot}$ and with the initial helium abundance $Y = 0.28$. The initial abundance of elements heavier than helium was assumed to be the same as the solar metallicity $Z = 0.014$ (Asplund et al. 2009).

Evolutionary computations were performed using the MESA program version r15140 (Paxton et al. 2019). Convective mixing was treated following Böhm-Vitense (1958) with the mixing length to pressure scale height ratio $\alpha_{\text{MLT}} = 1.8$. Extra mixing at boundaries of convection zones was calculated according to Herwig (2000) with overshooting parameter values recommended by Pignatari et al. (2016). The equations of nucleosynthesis were solved for the network consisting of 26 isotopes from hydrogen ^1H to magnesium ^{24}Mg . The rates of 81 nuclear reactions were calculated with the data base REACLIB (Cyburt et al. 2010). The mass loss rate at evolutionary stages prior to AGB was evaluated following to Reimers (1975) with the parameter $\eta_{\text{R}} = 0.5$, whereas in calculations of the AGB stage the mass loss rate was computed according to Bloeker (1995) with the parameter $\eta_{\text{B}} = 0.05$.

3 EVOLUTIONARY SEQUENCES FOR R HYA

Fig. 1 shows the duration of time intervals as a function of the number of the thermal pulse i_{TP} for evolutionary sequences $1.5M_{\odot} \leq M_{\text{ZAMS}} \leq 4.7M_{\odot}$. The plots corresponding to the first and second radius decline are shown by dashed and solid lines, respectively. As can be seen from these plots, to explain period decrease in R Hya we should consider the models of evolutionary sequences $1.5M_{\odot} \leq M_{\text{ZAMS}} \leq 2M_{\odot}$ for thermal pulses $4 \lesssim i_{\text{TP}} \lesssim 11$ (first radius decline) and $M_{\text{ZAMS}} \geq 4.7M_{\odot}$ for $i_{\text{TP}} \gtrsim 5$ (second radius decline).

To determine the applicability of evolutionary sequences $1.5M_{\odot} \leq M_{\text{ZAMS}} \leq 2M_{\odot}$ for explanation of period decrease in R Hya we calculated the pulsation periods at maxima

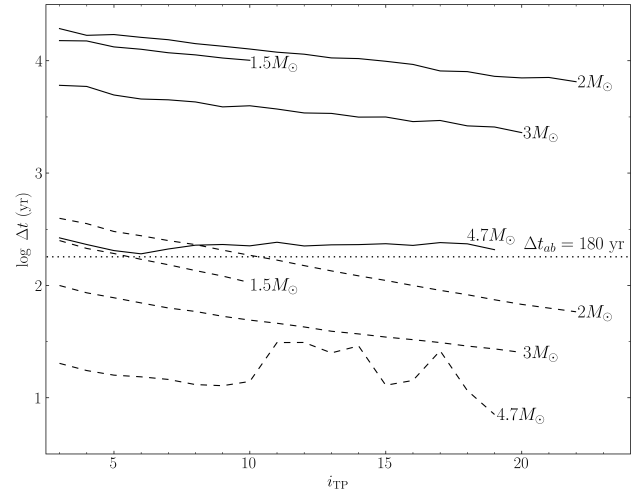


Figure 1. Duration of the first (dashed lines) and second (solid lines) radius decline as a function of the number of thermal pulse i_{TP} . The initial mass M_{ZAMS} is indicated at the curves. The dotted line represent the time interval $\Delta t_{ab} = 180$ yr.

of the helium-burning shell luminosity corresponding to the onset of first radius decline. To this end we computed the self-excited radial oscillations (see below section 4) and evaluated the period after attainment of limiting amplitude. Results of pulsation computations for evolutionary sequences $M_{\text{ZAMS}} = 1.5M_{\odot}$, $1.8M_{\odot}$ and $2M_{\odot}$ are shown in Fig. 2, where the filled circles and triangles represent the pulsation periods corresponding to the fundamental mode and the first overtone. Fundamental mode periods of three hydrodynamic models that were found to be stable against radial oscillations are shown in Fig. 2 by open circles.

As seen in Fig. 2, the fundamental mode periods of evolutionary sequences $1.5M_{\odot} \leq M_{\text{ZAMS}} \leq 2M_{\odot}$ are significantly smaller than the period $\Pi_a \approx 480$ d corresponding to the onset of period decrease in R Hya. Therefore, any stellar models with period decrease during the first radius decline can be rejected from further consideration.

Evolutionary calculations by Vassiliadis & Wood (1993) show that the luminosity and radius time dependencies of some thermally pulsing AGB star models exhibit the bump during the second radius decline. The bump (or the secondary maximum) is due to the thermal wave of the helium-shell flash that reflects from the star’s center. This feature is illustrated in Fig. 3, where the temporal dependences of the stellar radius in the models of the evolutionary sequence $M_{\text{ZAMS}} = 1.8M_{\odot}$ are shown for thermal pulses $i_{\text{TP}} = 6, 8$ and 10 . For the sake of convenience, the time t_{ev} in these plots is set to zero at the maximum peak luminosity $L_{3\alpha}$ of the helium-shell flash.

As seen in Fig. 3, the time interval between the maximum radius and the local radius minimum prior to the bump is much shorter than that of the second radius decline. Therefore, one could attempt to construct the model with temporary cessation of radius decline in order to reconcile observations of R Hya with theoretical estimates of the pulsation period at the maximum radius and the period decrease duration.

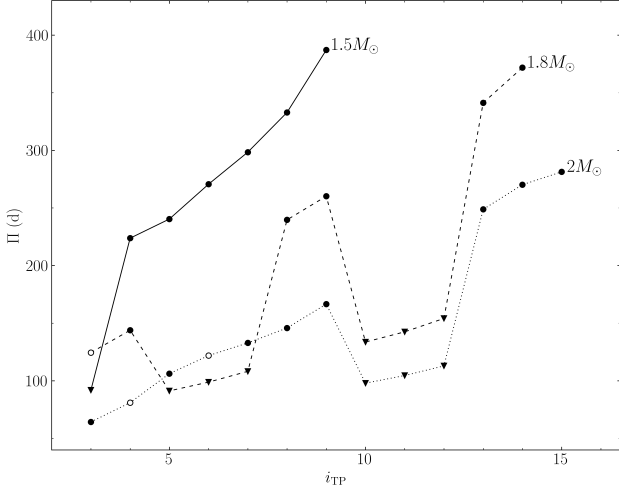


Figure 2. The pulsation period at the onset of radius decline as a function of the number of thermal pulse i_{TP} for evolutionary sequences $M_{\text{ZAMS}} = 1.5M_{\odot}$, $1.8M_{\odot}$ and $2M_{\odot}$. Filled circles and triangles correspond to the pulsation instability in the fundamental mode and first overtone. Open circles show fundamental mode periods of pulsationally stable models.

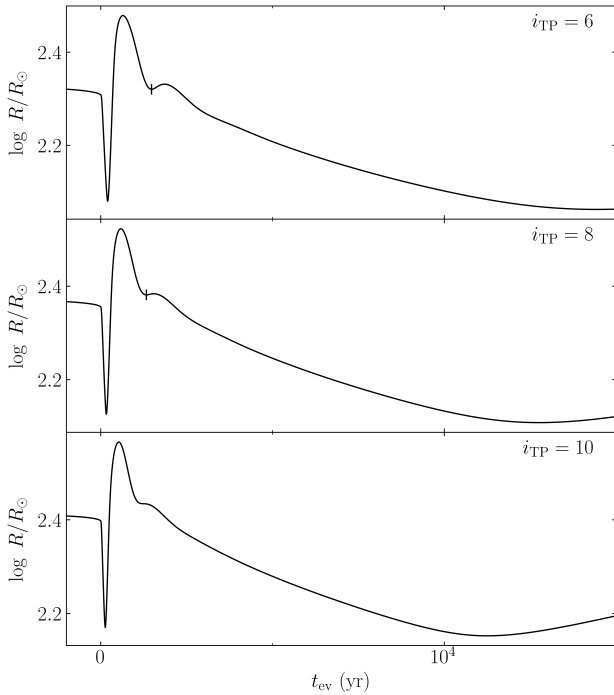


Figure 3. Time dependences of the stellar radius for the models of the evolutionary sequence $M = 1.8M_{\odot}$ during the thermal pulses $i_{\text{TP}} = 6, 8$ and 10 . Vertical ticks on the plots mark the local radius minimum prior to the secondary maximum of the radius.

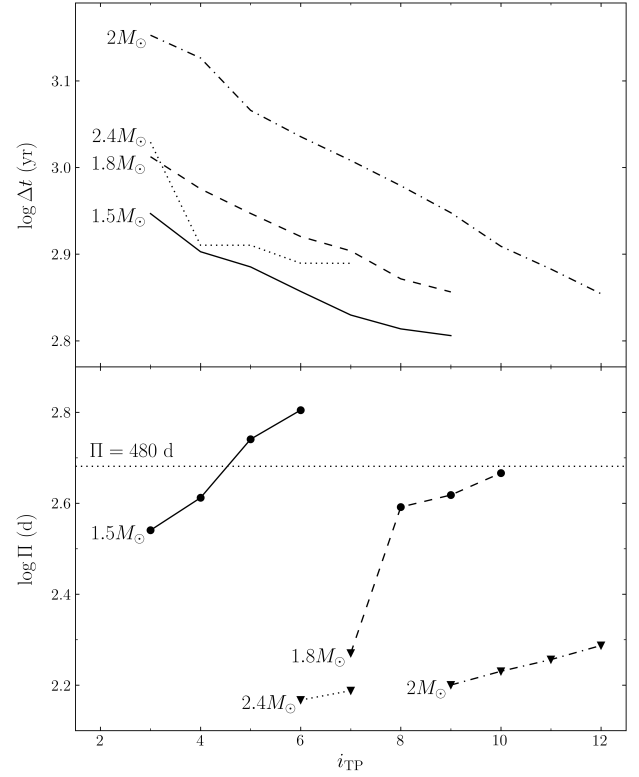


Figure 4. The time interval between the radius maximum and the local minimum due to the bump (upper panel) and the pulsation period at the maximum radius (lower panel) as a function of the number of thermal pulse i_{TP} . Filled circles and triangles represent the fundamental mode and first overtone pulsators, respectively.

In the present study the bump during the second radius decline was found in the evolutionary sequences with initial masses $1.5M_{\odot} \leq M_{\text{ZAMS}} \leq 2.4M_{\odot}$. Both the duration of the radius decline and the time interval between the maximum radius and the local radius minimum prior to the bump Δt decrease as the star evolves and the carbon core mass grows. Plots of the length of the time interval Δt as a function of the number of thermal pulse i_{TP} are shown in the upper panel of Fig. 4. As seen in Fig. 3, the amplitude of the bump reduces with increasing i_{TP} so that finally the secondary maximum transforms into the bump with monotonic decline of the radius where only the second time derivative of the radius changes the sign. The end-points of the plots in the upper panel of Fig. 4 correspond to the last secondary maximum before its disappearance during the following thermal pulse. The lower limit of the time interval ranges from $\Delta t = 640$ yr for $M_{\text{ZAMS}} = 1.5M_{\odot}$ to $\Delta t = 780$ yr for $M_{\text{ZAMS}} = 2.4M_{\odot}$.

Envelopes of the stellar models at the maximum radius after the helium flash are under thermal equilibrium and their pulsation periods we evaluated using the computational procedure described above. Because in each evolutionary sequence the time interval Δt decreases monotonically with increasing i_{TP} , of most interest are the pulsation models in the vicinity of the end-point of the plots in the upper panel of Fig. 4.

Results of pulsation calculations are presented in the lower

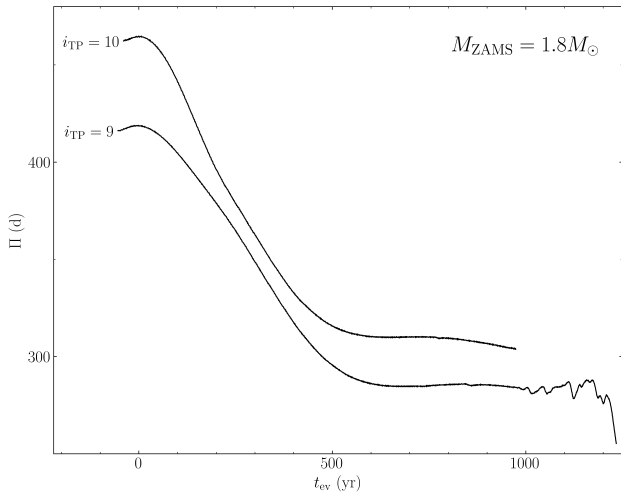


Figure 5. Evolution of the pulsation period in the hydrodynamic models of the evolutionary sequence $M_{\text{ZAMS}} = 1.8M_{\odot}$ at thermal pulses $i_{\text{TP}} = 9$ and $i_{\text{TP}} = 10$.

panel of Fig. 4. In the evolutionary sequence $M_{\text{ZAMS}} = 1.5M_{\odot}$ the model corresponding to $i_{\text{TP}} = 6$ pulsates in the fundamental model with period $\Pi = 550$ d whereas the time interval between the radius maximum and the local minimum due to the bump is $\Delta t = 770$ yr. On the other hand, the models of evolutionary sequences $M_{\text{ZAMS}} = 2M_{\odot}$ and $M_{\text{ZAMS}} = 2.4M_{\odot}$ pulsate in the first overtone with periods shorter than 200 d.

Thus, an assumption that the period decrease in R Hya occurred during the second radius decline from the maximum radius to the local radius minimum prior to the secondary maximum is not compatible with the twin requirements that the maximum pulsation is about 480 d and the duration of period decline lasts only about 180 yr. To confirm this conclusion we can consider the model of the evolutionary sequence $M_{\text{ZAMS}} = 1.8M_{\odot}$ with period at the maximum stellar radius $\Pi_a = 465$ d ($i_{\text{TP}} = 10$) which has less deviation from the period value $\Pi_a^* = 480$ d. As seen in the lower panel of Fig. 3, the secondary maximum in the plot for this model disappears but location of the bump in the plot nearly corresponds to the time interval $\Delta t \approx 700$ yr.

Fig. 5 presents time variations of the pulsation period $\Pi(t_{\text{ev}})$ during radius decline for the thermal pulses $i_{\text{TP}} = 9$ and $i_{\text{TP}} = 10$ in the evolutionary sequence $M_{\text{ZAMS}} = 1.8M_{\odot}$. To obtain these dependencies we solved the initial-value problem for equations of hydrodynamics with the inner boundary conditions determined from evolutionary models. The method of calculations is described in Fadeyev (2022).

As seen from plots in Fig. 5, the duration of the period decrease is $\Delta t \approx 500$ yr. The pulsation period during the temporary cessation of the radius decline ($600 \text{ yr} \lesssim t_{\text{ev}} \lesssim 800 \text{ yr}$) is $\Pi_b = 310$ d and the period ratio $\Pi_a/\Pi_b = 1.50$ is significantly larger than that in R Hya ($\Pi_a^*/\Pi_b^* = 1.26$). Thus, the AGB star models with initial mass $M_{\text{ZAMS}} < 3M_{\odot}$ cannot be reconciled with observations of R Hya and therefore we have to consider the models of more massive stars.

As was shown in our previous paper (Fadeyev 2023), the duration of the second radius decline Δt_{ab} deviates less from

Table 1. Duration of the second contraction phase in thermal pulses $4 \leq i_{\text{TP}} \leq 9$ of evolutionary sequences $4.5M_{\odot} \leq M_{\text{ZAMS}} \leq 5.0M_{\odot}$.

M_{ZAMS} M_{\odot}	4	5	Δt_{ab} (yr)			
			6	7	8	9
4.5	295	257	234	226	260	268
4.6	243	228	209	218	248	257
4.7	231	204	191	211	228	231
4.8	219	197	173	189	188	187
4.9	206	171	151	182	182	185
5.0	195	160	153	157	155	157

the duration of period decrease in R Hya for models of the evolutionary sequence with initial mass $M_{\text{ZAMS}} \approx 4.8M_{\odot}$. Results of more detailed calculations carried out in the present study are summarized in Table 1, where the values of Δt_{ab} corresponding to the thermal pulses $4 \leq i_{\text{TP}} \leq 9$ are given for models of evolutionary sequences $4.5M_{\odot} \leq M_{\text{ZAMS}} \leq 5.0M_{\odot}$. As seen in Table 1, the duration of the second contraction phase decreases with increasing stellar mass and is insignificantly sensitive to i_{TP} . Bearing in mind that the duration of period decrease in R Hya is $\Delta t_{ab}^* \approx 180$ we can conclude that the initial masses of the most appropriate evolutionary sequences are $4.7M_{\odot} \leq M_{\text{ZAMS}} \leq 4.9M_{\odot}$.

The time-dependent inner boundary conditions are illustrated in Fig. 6. The upper panel of Fig. 6 shows the temporal variation of the surface radius of the evolutionary model R in the time interval spanned by hydrodynamic computations for the model of the evolutionary sequence $M_{\text{ZAMS}} = 4.8M_{\odot}$ during the 4-th thermal pulse. For the sake of convenience the evolution time t_{ev} is set to zero at the maximum peak luminosity $L_{3\alpha}$ of the helium-shell flash. The inner boundary of the hydrodynamic model is set at the Lagrangean mass coordinate $M_0 = 0.187M$, where $M = 4.605M_{\odot}$ is the mass of the AGB star model. The time-dependent inner boundary conditions $r_0(t_{\text{ev}})$ and $L_0(t_{\text{ev}})$ are determined by non-linear interpolation with respect to the mass coordinate M_r and are shown in the middle and bottom panels, respectively. The dashed line in the bottom panel represents the surface luminosity of the evolution model.

The most striking feature in Fig. 6 is the presence of oscillations of the inner boundary luminosity $L_0(t_{\text{ev}})$ during expansion of the envelope within the time interval $15 \text{ yr} \lesssim t_{\text{ev}} \lesssim 90 \text{ yr}$. These oscillations arise due to both the small-amplitude variations of the energy released by hydrogen burning and the close location of the inner boundary to the hydrogen-shell source. For example, in the model shown in Fig. 6 the mass difference between the hydrogen-shell source and the inner boundary is $\delta M_r \sim 10^{-3}M_{\odot}$. To diminish the amplitude of oscillations in L_0 we carried out the evolutionary computations with the larger number of mass zones N . The plot in the lower panel of Fig. 6 corresponds to $N \approx 8 \times 10^4$ so that oscillations of L_0 with amplitude $\delta L_0/L_0 \lesssim 10\%$ do not affect the surface luminosity.

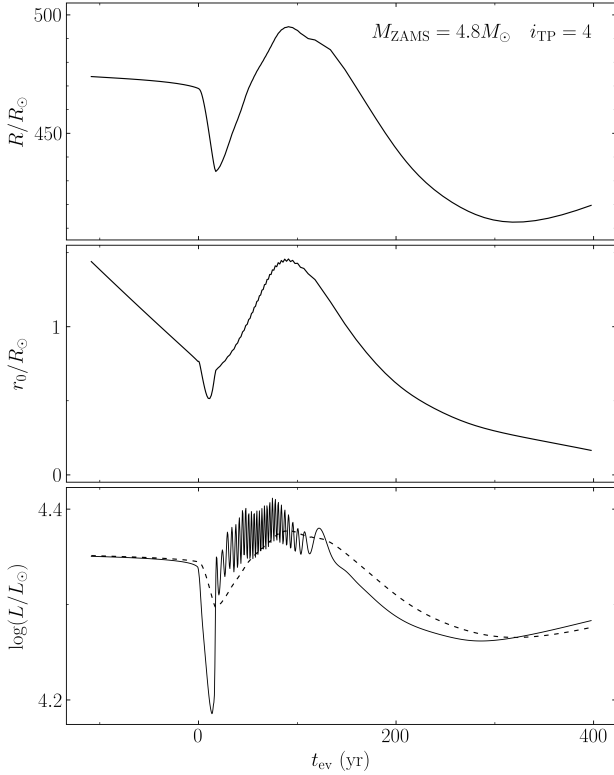


Figure 6. Variations with time of the surface radius R (upper panel) and the radius at the inner boundary r_0 (middle panel) for the evolutionary sequence $M_{\text{ZAMS}} = 4.8M_{\odot}$ during the thermal pulse $i_{\text{TP}} = 4$. In the bottom panel, the inner boundary condition L_0 (solid line) and the stellar luminosity L (dashed line) as a function of the age t_{ev} .

4 INITIAL CONDITIONS FOR HYDRODYNAMIC MODELS

Calculations of hydrodynamic stellar models with evolving pulsation period are done using the initial conditions in the form of the limiting amplitude stellar pulsation model computed with the time-independent inner boundary conditions

$$\frac{\partial r_0}{\partial t} = \frac{\partial L_0}{\partial t} = 0. \quad (1)$$

The necessary condition for correct application of the theory of stellar pulsation is that the evolutionary stellar model is under hydrostatic and thermal equilibrium. All models of evolutionary sequences are under hydrostatic equilibrium and at the same time may be in thermal imbalance during stellar contraction or expansion. Therefore, the selection of appropriate evolutionary models should be based on the estimate of the deviation from thermal equilibrium. For the spherically symmetric stellar envelope without nuclear energy sources the deviation from thermal equilibrium can be expressed as

$$\delta_L = \max_{1 \leq j \leq N} |1 - L_j/L_0|, \quad (2)$$

where L_j is the total (radiative plus convective) luminosity at the j -th mass zone, L_0 is the luminosity at the inner boundary, N is the number of mass zones in the hydrodynamic

model. Evolution models with the age $t_{\text{ev}} \approx -100$ yr, where $t_{\text{ev}} = 0$ at the maximum peak luminosity $L_{3\alpha}$, were found to satisfy the condition $\delta_L \lesssim 10^{-3}$ corresponding to negligible thermal imbalance in the stellar envelope.

The Lagrangean mesh of the initial hydrodynamic model was determined for the outer layers with the radius at the innermost mass zone $r_0 \sim 10^{-3}R$, where R is the radius of the outer boundary of the evolution model. All hydrodynamic models were computed with $N = 900$ mass zones, where the mass intervals of 800 outer zones increase geometrically inwards whereas the mass intervals of 100 inner zones decrease. This approach allowed us to obtain a better approximation in the inner layers of the stellar envelope where the pressure and temperature gradients sharply change. The variables specified on the Lagrangean mesh of the initial hydrodynamic model were evaluated using the non-linear interpolation of stellar evolution model data with respect to the mass coordinate M_r .

To calculate the self-excited non-linear stellar oscillations we solved the equations of radiation hydrodynamics and time-dependent convection where the transport equations for convective mixing were used in the form by Kuhfuss (1986). The full system of the equations of hydrodynamics and the choice of parameters are discussed in our preceding paper (Fadeyev 2015).

Results of calculations of the self-excited radial oscillations with static inner boundary conditions are illustrated in Figs. 7 and 8 for two models of the evolutionary sequence $M_{\text{ZAMS}} = 4.8M_{\odot}$ prior to the thermal pulses $i_{\text{TP}} = 4$ and $i_{\text{TP}} = 7$, respectively. The plots in the left and right sections of the figures correspond to the stages prior to and after attainment of limiting amplitude. In upper panels we give the plots of the maximum values of the kinetic energy $E_{\text{K,max}}$ which is reached twice per pulsation period. Both models have the close values of periods and growth rates: $\Pi = 441$ d, $\eta = \Pi d \ln E_{\text{K,max}}/dt = 0.11$ for $i_{\text{TP}} = 4$ and $\Pi \approx 459$ d, $\eta = 0.12$ for $i_{\text{TP}} = 7$ but at the same time they demonstrate different behaviour after the limiting amplitude attainment. This due to the fact that R Hya models are at the edge between the regular and numerically over-driven stellar pulsations.

Attainment of the limiting amplitude occurs not only due to saturation of the κ -mechanism in the hydrogen ionization zone but also because of kinetic energy dissipation by shock waves. The latter mechanism becomes significant at the large-amplitude oscillations. Moreover, periodic shock waves accompanying non-linear stellar pulsations are responsible for distension of the stellar envelope (Willson 2000). As seen in Figs. 4 and 5, the radial amplitude at the outer boundary is $\Delta R/R \approx 0.5$ whereas the ratio of the mean radius of the pulsating star to the radius of the evolution model is $\bar{R}/R_{\text{ev}} \approx 1.1$. The lack of any secular change in the mean radius \bar{R} indicates the absence of entropy changes arising due to the thermal imbalance in the initial stellar model (Ya'Ari & Tuchman 1996).

5 EVOLUTION OF THE PULSATION PERIOD

Solution of the radiation hydrodynamics equations based on the time-dependent inner boundary conditions is almost consistent with results of stellar evolution computations. The

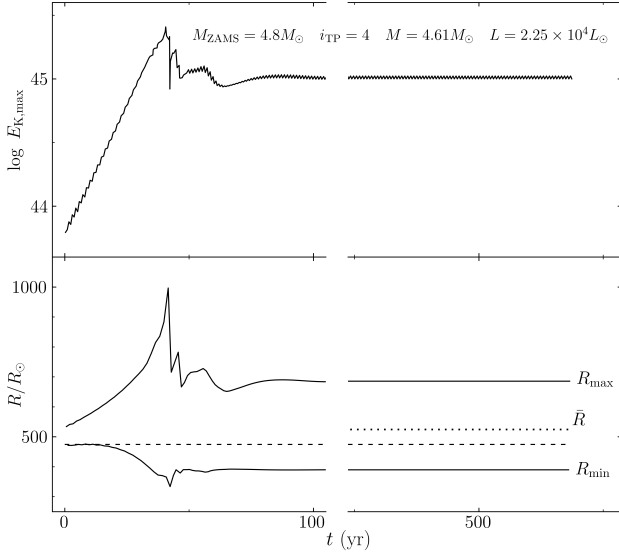


Figure 7. The maximum kinetic energy $E_{K,\max}$ versus time t (top panel) for the hydrodynamic model of the evolutionary sequence $M_{ZAMS} = 4.8M_{\odot}$ prior to the thermal pulse $i_{TP} = 4$. In the bottom panel, the maximum and minimum radii R_{\max} and R_{\min} of the outer boundary of the hydrodynamic model (solid lines). The dotted and dashed lines represent the mean radius over the pulsation period \bar{R} and the radius of the evolution model, respectively.

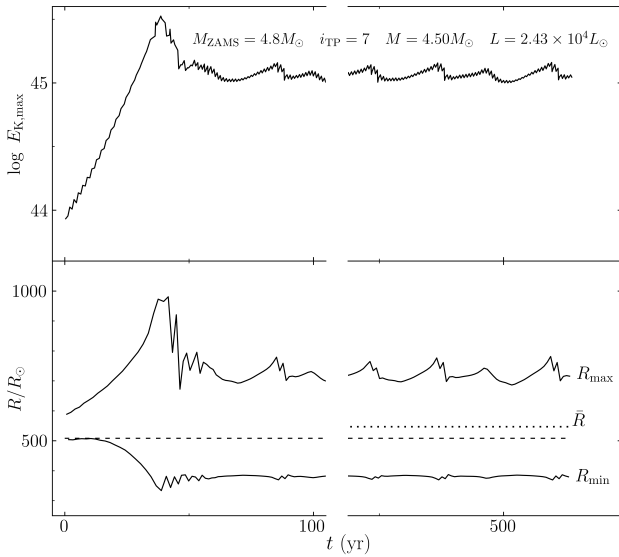


Figure 8. Same as Fig. 7, but for the hydrodynamic model prior to the thermal pulse $i_{TP} = 7$.

only exception is that the non-linear stellar pulsations are calculated for the constant mass of the hydrodynamic model, whereas the mass of the evolution model gradually decreases. However hydrodynamic computations are carried out for time intervals as long as 500 yr so that the mass difference between the evolutionary and hydrodynamic models is negligible and does not exceed 0.1%.

The top panel of Fig. 9 shows the maximum and the min-

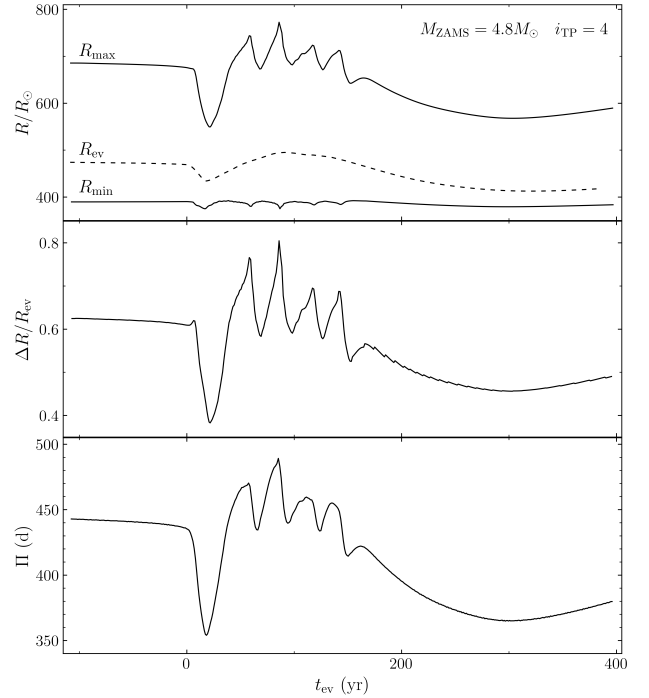


Figure 9. Upper panel: variation with evolution time t_{ev} of maximum and minimum radii of the hydrodynamic model with initial mass $M_{ZAMS} = 4.8M_{\odot}$ during the thermal pulse $i_{TP}=4$ (solid lines). The dashed line shows the time variation of the surface radius of the evolution model. Middle and bottom panels: the pulsation amplitude and pulsation period versus evolution time.

imum radii R_{\max} and R_{\min} as a function of evolution time t_{ev} for the hydrodynamic model corresponding to the evolutionary sequence $M_{ZAMS} = 4.8M_{\odot}$ during the thermal pulse $i_{TP} = 4$. The dashed line in the upper panel represents the temporal variation of the radius R_{ev} of the evolution model.

The middle panel of Fig. 9 shows the pulsation amplitude at the outer boundary of the hydrodynamic model ΔR expressed in units of R_{ev} . As can be seen, the radial pulsations become numerically over-driven near the maximum of R_{ev} within the time interval $30 \text{ yr} \lesssim t_{ev} \lesssim 170 \text{ yr}$ when the radiation diffusion wave generated by the helium-shell flash reaches the convection envelope of the pulsating star and the pulsation amplitude becomes as large as $\Delta R > 0.7R_{ev}$.

Semi-regular variations of Π with the amplitude $\lesssim 10\%$ and the cycle length ranging from 20 to 30 yr (the bottom panel of Fig. 9) are due to the large-amplitude changes of the stellar radius because the pulsation period Π is nearly proportional to $R^{3/2}$. It should be noted that all hydrodynamic models computed in the present study exhibit the similar behaviour of the pulsation period.

Of most interest for comparison with observations of R Hya is the time interval spanning over ≈ 200 yr between the maximum and minimum values of the period. Fig. 10 shows the temporal dependencies of the pulsation period for hydrodynamic models of the evolutionary sequences $M_{ZAMS} = 4.7M_{\odot}$, $4.8M_{\odot}$ and $4.9M_{\odot}$ during the thermal pulses $4 \leq i_{TP} \leq 7$. In each panel of this figure we plot observational estimates of the period from Prager (1936), from the light

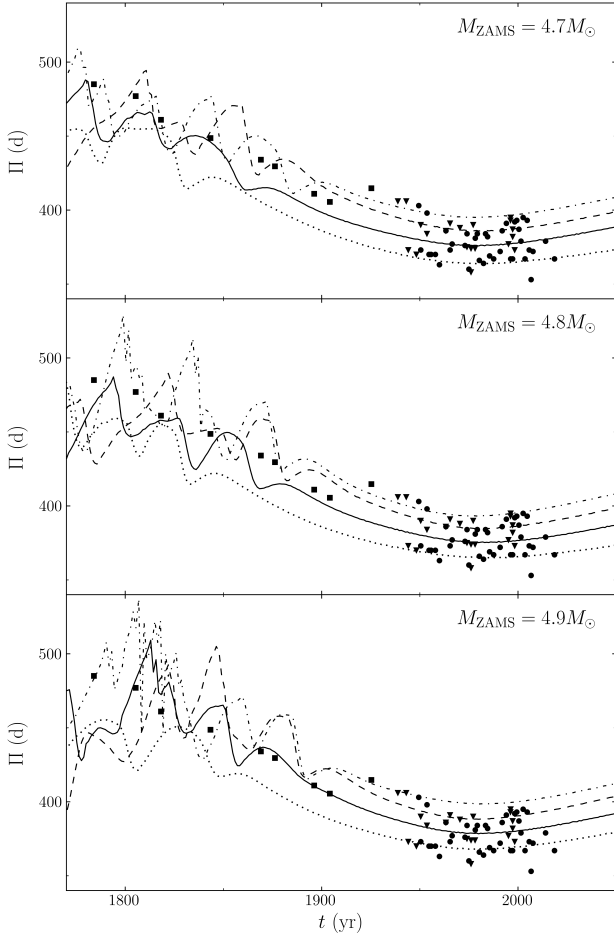


Figure 10. Pulsation period as a function of time for evolutionary sequences $M_{\text{ZAMS}} = 4.7M_{\odot}$, $4.8M_{\odot}$ and $4.9M_{\odot}$ for thermal pulses $i_{\text{TP}} = 4$ (dotted lines), $i_{\text{TP}} = 5$ (solid lines), $i_{\text{TP}} = 6$ (dashed lines) and $i_{\text{TP}} = 7$ (dashed-dotted lines). Observational estimates of the period for R Hya are plotted with filled squares (Prager 1936), filled circles (using light curve data taken from AAVSO) and filled triangles (from the card catalogue of variable stars of the Sternberg Astronomical Institute).

curve data base of the AAVSO and from the card catalogue of variable stars of the Sternberg Astronomical Institute.

It should be noted that in order to compare the results of computations with observations we arbitrarily shifted the plots of $\Pi(t)$ along the horizontal axis and as can be seen in Fig. 10, the best agreement with observations is obtained for the minimum of $\Pi(t)$ in ≈ 1980 . At the same time one should bear in mind that the localization of the period minimum is quite uncertain because of very slow period change near the minimum. For example, decrease of the period dependence $\Pi(t)$ before its minimum be nearly 5% takes place during nearly 70 yr.

Hydrodynamic models of evolutionary sequences represented in Fig. 10 are not very sensitive to the initial stellar mass M_{ZAMS} but at the same time show a notable dependence on the number of the thermal pulse i_{TP} because of the gradually increasing radius and luminosity as a star evolves

Table 2. Parameters of hydrodynamic models at the minimum pulsation period Π_b .

M_{ZAMS} M_{\odot}	i_{TP}	$\dot{\Pi}$ d yr^{-1}	M M_{\odot}	L $10^4 L_{\odot}$	R_{ev} R_{\odot}	\bar{R} R_{\odot}	Π_b d	C/O
4.7	5	-0.57	4.50	1.84	410	469	364	0.38
4.7	6	-0.53	4.43	1.88	427	486	386	0.42
4.8	5	-0.70	4.58	1.88	422	482	375	0.37
4.8	6	-0.42	4.54	1.92	430	489	385	0.40
4.9	5	-0.57	4.67	1.95	428	487	378	0.37
4.9	6	-0.36	4.64	1.99	436	495	388	0.40

along AGB. As can be seen in 10, the best agreement with observations is obtained for $5 \leq i_{\text{TP}} \leq 6$.

Parameters of hydrodynamic models that agree with observations age listed in Table 2, where in the third column we give the average period change rate $\dot{\Pi}$ evaluated by the linear fit of $\Pi(t)$ within the time interval $1780 \leq t \leq 1950$. During the same time interval the period of R Hya declined almost linearly with rate $\approx -0.58 \text{ d yr}^{-1}$ (Zijlstra et al. 2002).

The mass M , luminosity L and radius R_{ev} of the evolution model given in Table 2 correspond to the phase of the minimum pulsation period Π_b . The significant difference between the average radius of the hydrodynamic model \bar{R} and the radius of the evolution model R_{ev} is due to distension of the stellar envelope because of periodic shock waves accompanying the large-amplitude oscillations. In the last column of Table 2 we give the surface carbon-to-oxygen number ratio C/O. Just before the first helium-shell flash this ratio is C/O=0.33 for all evolutionary sequences so that the computed hydrodynamic models represent the oxygen-rich Mira-type stars at the beginning of the third dredge-up.

6 CONCLUSIONS

Solution of the radiation hydrodynamics equations with time-dependent inner boundary conditions allows us to conclude that nearly 200 years ago the amplitude of stellar oscillations in R Hya reached the maximum value due to substantial increase in the both surface radius and luminosity. The large-amplitude stellar oscillations give rise to the shock wave driven mass loss and it is of interest to note that during decline of the stellar radius, luminosity and pulsation amplitude between 1770 and 1950 the mass loss rate decreased by a factor of ≈ 20 (Decin et al. 2008). Moreover, the large-amplitude pulsations taking place two centuries ago seem to be responsible for the formation of the cold dust shell surrounding R Hya (Hashimoto et al. 1998).

As seen in Fig. 7, a major disagreement between the calculated temporal dependencies of the pulsation period $\Pi(t)$ and observational period estimates for R Hya corresponds to observations conducted earlier than 1900 when the pulsation amplitude was significantly larger than nowadays. Unfortunately, the large-amplitude oscillations of the hydrodynamic models cannot be corroborated by observations of R Hya because they were rare and inexact.

Observations of R Hya are well fitted with the temporal dependencies calculated for the hydrodynamic models of the evolutionary sequence $M_{\text{ZAMS}} = 4.7M_{\odot}$ during the thermal pulses $i_{\text{TP}} = 5$ and $i_{\text{TP}} = 6$. Moreover, the mean radius of

this hydrodynamic model near the minimum of the period (see Table 2) has the least deviation from the observational estimate of the radius $R = 442R_{\odot} \pm 65R_{\odot}$ obtained from interferometric angular diameter measurements of R Hya (Haniff et al. 1995).

ACKNOWLEDGEMENTS

The author is indebted to amateur astronomers of the AAVSO for their observations of R Hydrae. The author also expresses his gratitude to Prof. N.N. Samus', the head of the GCVS Research Group of the Sternberg Astronomical Institute, for his help in accessing the historical card catalogue of variable stars. The author is grateful to the anonymous referee for his meticulous review of this paper and the valuable comments.

DATA AVAILABILITY

The data underlying this article will be shared on reasonable request to the corresponding author.

REFERENCES

- Argelander F. W. A., 1869, *Astronomische Beobachtungen auf der Sternwarte zu Bonn*, **7**, 315
- Asplund M., Grevesse N., Sauval A. J., Scott P., 2009, *ARA&A*, **47**, 481
- Bloecker T., 1995, *A&A*, **297**, 727
- Böhm-Vitense E., 1958, *Z. Astrophys.*, **46**, 108
- Boothroyd A. I., Sackmann I. J., 1988, *ApJ*, **328**, 632
- Chandler S. C., 1896, *AJ*, **16**, 145
- Cyburt R. H., et al., 2010, *ApJS*, **189**, 240
- Decin L., Blomme L., Reyniers M., Ryde N., Hinkle K. H., de Koter A., 2008, *A&A*, **484**, 401
- Fadeyev Y. A., 2015, *MNRAS*, **449**, 1011
- Fadeyev Y. A., 2022, *MNRAS*, **514**, 5996
- Fadeyev Y. A., 2023, *Astronomy Letters*, **49**, 167
- Gould B. A., 1882, *Astronomische Nachrichten*, **102**, 341
- Haniff C. A., Scholz M., Tuthill P. G., 1995, *MNRAS*, **276**, 640
- Hashimoto O., Izumiura H., Kester D. J. M., Bontekoe T. R., 1998, *A&A*, **329**, 213
- Herwig F., 2000, *A&A*, **360**, 952
- Iben I. J., 1982, *ApJ*, **260**, 821
- Kuhfuss R., 1986, *A&A*, **160**, 116
- Lebzelter T., Hron J., 2003, *A&A*, **411**, 533
- Little S. J., Little-Marenin I. R., Bauer W. H., 1987, *AJ*, **94**, 981
- Merrill P. W., 1946, *ApJ*, **103**, 6
- Merrill P. W., 1952, *ApJ*, **116**, 18
- Merrill P. W., 1957, *PASP*, **69**, 77
- Müller G., Hartwig E., 1922, *Geschichte und Literatur des Lichtwechsels, der bis Ende 1915 als sicher veränderlich anerkannten Sterne: nebst einem Katalog der Elements ihres Lichtwechsels*. Leipzig
- Orlov M. Y., Shavrina A. V., 1984, *Nauchnye Informatsii*, **56**, 97
- Paxton B., et al., 2019, *ApJS*, **243**, 10
- Pignatari M., et al., 2016, *ApJS*, **225**, 24
- Prager R., 1936, *Geschichte und Literatur der Lichtwechsels der veränderliche Sterne. Zweite Ausgabe enthaltend die Literatur der Jahre 1916-1933*. Berlin
- Reimers D., 1975, in , *Problems in stellar atmospheres and envelopes..* pp 229–256
- Samus' N. N., Kazarovets E. V., Durlevich O. V., Kireeva N. N., Pastukhova E. N., 2017, *Astronomy Reports*, **61**, 80
- Vassiliadis E., Wood P. R., 1993, *ApJ*, **413**, 641
- Willson L. A., 2000, *ARA&A*, **38**, 573
- Wood P. R., Zarro D. M., 1981, *ApJ*, **247**, 247
- Ya'Ari A., Tuchman Y., 1996, *ApJ*, **456**, 350
- Zijlstra A. A., Bedding T. R., Mattei J. A., 2002, *MNRAS*, **334**, 498

This paper has been typeset from a $\text{\TeX}/\text{\LaTeX}$ file prepared by the author.